Ultrasonics Sonochemistry 84 (2022) 105962

Contents lists available at ScienceDirect

Ultrasonics Sonochemistry

journal homepage: www.elsevier.com/locate/ultson

Effect of ultrasound pre-treatment on carbonaceous copper-bearing shale flotation

Mateusz Kruszelnicki [a,*], Ahmad Hassanzadeh [b,c,*], Krzysztof Jan Legawiec [a], Izabela Polowczyk [a], Przemyslaw B. Kowalczuk [b]

[a] Wroclaw University of Science and Technology, Department of Process Engineering and Technology of Polymer and Carbon Materials, Wybrzeze Wyspianskiego 27, Wroclaw 50-370, Poland
[b] NTNU Norwegian University of Science and Technology, Department of Geoscience and Petroleum, Andersens veg 15a, 7031 Trondheim, Norway
[c] Maelgwyn Mineral Services Ltd, Ty Maelgwyn, 1A Gower Road, Cathays, Cardiff CF24 4PA, United Kingdom

ARTICLE INFO

Keywords:
Ultrasound-assisted flotation
Copper-bearing shale
Pre-treatment
Ultrafine bubbles
Particle surface charge

ABSTRACT

Although numerous studies have been implemented on identifying the impact of acoustic waves on mineral beneficiation, its fundamental aspects remain unclear in the literature. The present work, for the first time, systematically investigates the role of ultrasound pre-treatment (UPT) in the carbonaceous copper-bearing shale flotation. To this end, conditioning was carried out at different powers of applied ultrasound. Non-treated and UPT shale flotation tests were performed in the presence of frother (MIBC) and collector (KEX). To analyse particle surface charge variation and collector adsorption properties after application of UPT, zeta potential and ultraviolet–visible spectroscopy measurements were implemented, respectively. The generation of sub-micron bubbles due to the acoustic cavitation was characterised by laser-based particle size measurements. Shale hydrophobicity was determined using the sessile drop and captive bubble techniques.

The micro-flotation results showed that the mass recovery increased by 40% at 20 W of applied ultrasonic power. The positive effect of UPT on the copper-bearing shale flotation was related to: i) generation of ultrafine bubbles due to the acoustic cavitation phenomenon and ii) the cleaning effect through transient bubble collapse. However, rigorous ultra-sonication diminished the recoverability of the sample owing to the less intensified number of ultrafine bubbles on the particle surfaces and formation of free H and OH radicals, which led to the oxidation of particle surfaces. These statements were correlated well with the observations of the zeta potential, particle size analysis and quantified ultrafine bubbles. Finally, we briefly highlighted fundamental knowledge gaps in flotation and ultrasound-related issues for future work.

1. Introduction

Through ultrasonic wave propagation in a slurry, the environment undergoes physical and chemical changes. This results in a series of mechanical, thermal, electromagnetic, and chemical ultrasonic effects including cavitation and sonochemistry. An acoustic cavitation phenomenon induces an increase in medium temperature, promotes mass transfer and produces ultrafine bubbles through three steps as (i) formation of cavitation bubbles, (ii) growth, and then (iii) implosive collapse [1]. A sonochemical impact of ultrasound is mainly related to the implosion of fine bubbles and the generation of free radicals with a great propensity for reaction. This property of acoustic waves is more dominant at intermediate frequencies as the number of produced active bubbles is adequately high and mainly controlled by temperature and power of sonication [2].

Over the last three decades, acoustic waves have been widely applied to the froth flotation either as pre-treatment [3,4] or a simultaneous process [5] to improve mineral floatability, increase flotation kinetics rate and reduce reagent consumptions. Its positive effects are extensively argued in the literature based on cleaning and removing slime coatings [4,6], creation of ultrafine air bubbles through ultrasonic cavitation phenomenon [7], facilitating superior collector adsorption [8], generation of H and OH radicals [9], enhancement of contact angle [10], and modification of medium properties, including pH, temperature, dissolved oxygen, and conductivity [11]. In addition to the ultrasonic treatment methods, i.e., pre-conditioning and flotation [12], the

* Corresponding authors.
E-mail addresses: mateusz.kruszelnicki@pwr.edu.pl (M. Kruszelnicki), ahmad.hassanzadeh@ntnu.no (A. Hassanzadeh).

https://doi.org/10.1016/j.ultsonch.2022.105962
Received 20 November 2021; Received in revised form 21 February 2022; Accepted 23 February 2022
Available online 28 February 2022

local position of homogeniser's horn can cause either positive or negative effects on ultimate metallurgical responses (e.g., grade, recovery, separation efficiency, kinetics) [13,14]. Although its macroscopic aspects have been intimately investigated, little attention is given to its fundamental and particularly chemical impacts. For example, despite of common believe in formation of micro/nano bubbles under acoustic waves [15], Li et al. [16] showed that nanobubbles were not one of the outcomes for ultrasonication. Such contradiction plausibly originates from applying different experimental techniques and variation in the practical and measurement approaches.

Ultrasound power critically affects particle and medium properties through number of cavitated bubbles, elimination of oxidised or passivated layers, increase in H and OH radical quantities and solution temperature. Chen et al. [7] classified the ultrasonic effect into three groups, based on the frequency of applied ultrasound viz. low (20–50 kHz), medium (200–1000 kHz) and high (greater than 1 MHz). It was schematically demonstrated that at short acoustic times in the presence of low frequencies, slime coating and oxidation films can be removed from particle surfaces, while its prolongation was associated with the formation of free H and OH radicals and transient bubbles. To verify this, Cao et al. [17] reported the ultrasonication ($\geq$0.3 W/cm^2) effect on oxidised pyrite (by H_2O_2 solution for 12 min) and declared that ultrasound could induce surface cleaning at short-term durations (<20 s). However, above 20 s further oxidation was occurred due to the presence of H_2O_2 and nascent oxygen generated by the ultrasonic treatment. Following this, Hassanzadeh et al. [11] studied the wettability and collectorless (natural) floatability of chalcopyrite, pyrite, and quartz as a function of ultrasound power (0–180 W) at a constant acoustic pretreatment duration of 15 s. They found that although quartz and pyrite ultrasound-treated micro-flotation recoveries were lower than that of conventional ones, an optimum power level of 60–90 W was identified for maximising the chalcopyrite recovery. Aldrich and Feng [3] addressed similar results in case of a bulk base metal sulphide. They disclosed that after ultrasonic excitation, floatability of sulphides improved significantly, while the silicates were depressed to some extent. These case studies all provided invaluable information regarding the role of ultrasonication in froth flotation, however, none of them systematically evaluated the mineral or bulk materiaĺs flotation where this knowledge gap is filled out in the present work.

The impact of acoustic waves on the coal and graphite floatabilities has been extensively reported in the literature [4,16,18-21]. For instance, Li et al. [4] recovered clean coal from tailings using an ultrasonic-assisted flotation process (270 W, 10 min). The results showed that acoustic waves alleviated slime coating, decreased collector adsorption and increased combustible recovery of coal particles. Similar outcomes were stated by Ebrahimi and Karamoozian [22] who obtained 35%, 45% and 25% increase respectively in coarse (−800 + 400 μm), medium (−400 + 100 μm), and fine (<100 μm) fraction sizes by enhancing acoustic wavelength from 0 to 80 kHz. However, interestingly an ultrasonic bath unit was utilized in this work which normally operates in a range of power than in a controllable level. More recently, Xu et al., [23] indicated that recovery of fine graphite particles (d_{50} = 22 μm) was improved by about 12% in a Hallimond tube at 3.76% formation probability of surface microbubbles at 5 bar water. Kang and Li [21] concluded that ultrasonic treatment not only changed the size of flaky graphite, but also eliminated impurities on the graphite surface and improved its hydrophobicity. The yield, carbon content and recovery of flotation concentrate were respectively 5.83%, 2.86% and 8.84% greater in the presence of ultrasonic pre-treatment (4 min, 1600 W). The aim of this study is to investigate the effect of ultrasound pretreatment on the carbonaceous copper-bearing shale flotation. In addition to micro-flotation experiments, particle surface charge variation, the existence of acoustically created bubbles, adsorption properties and particle morphologies were evaluated in detail. To the best of author's knowledge, this is the first contribution to the in-depth analysis of ultrasonication impact in the froth flotation processes.

2. Materials and methods

2.1. Copper-bearing shale sample preparation and characterisation

A bulk sample of copper-bearing shale (hereinafter named as shale for short) originated from the Kupferscheifer stratiform copper deposit was collected from Polkowice-Sieroszowice mine (Lower Silesia, Poland). Since the key parameter in a conventional flotation process is the feed particle size distribution, which optimal size range is ca. 20–150 μm [24,25], the sample was first crushed in a Cross Beater Mill SK 300 (Retsch GmbH, Germany), and then a narrow size fraction of −125 + 80 μm was separated. Additionally, the −40 μm fraction was selected for zeta potential measurements in order to minimise particle settling in the measuring cell of the analyser, which could negatively influence the measurement results. The fractions were obtained by sieving material through a set of 125, 80 and 45 μm size sieves using a HAVER EML 200 digital sieve shaker (Haver & Boecker, Germany) with a screening time of 30 min at amplitude of 3 mm. The −125 + 80 μm fraction was additionally washed by sedimentation/decantation process to remove potential weakly attached finer particles. For this purpose, samples of 100 g were manually agitated in 1 L of water. Then, coarser particles were let to sediment, and the supernatant water with dispersed fine particles was carefully decanted. The procedure was repeated several times until no fine particles were observed in the liquid.

The chemical composition of the sample was determined by X-ray fluorescence (XRF, EDXRF PANalytical Epsilon 3X, USA). The average percentage contents of Cu, Ca, Fe, Zn, Al, Si and S were 6.0, 8.0, 11.8, 1.3, 0.3, 3.8, 10.6, and 1.7%, respectively. The investigated sample from the Polkowice-Sieroszowice mine corresponds to the P-KS-2 shale described by Rahfeld et al. [26], which was comprised of quartz (19%), sheet silicates (27%), carbonate minerals (38%), copper minerals (8%), other sulphides (<1%) and accessory minerals (6%). Fig. 1 shows the X-Ray diffraction (XRD) pattern of the sample recorded on D8 Advance diffractometer (Bruker, USA) with Cu Kα X-ray source (λ = 1.5406 Å) in the range 2θ = 10°–90°, with step 2θ = 0.008° and a step time of 1 s. Most intense diffraction peaks correspond to the aforementioned quartz, silicates and carbonate minerals.

2.2. Reagents

Commonly used flotation reagents for sulphide ore flotation [27] have been employed in this study and all were supplied by Sigma-

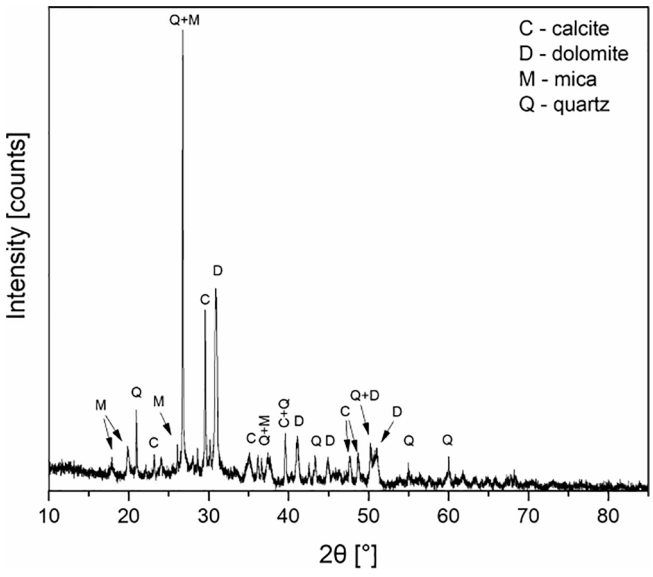

Fig. 1. X-Ray diffraction pattern of the studied shale sample.

Aldrich (Germany). Potassium ethyl xanthogenate (KEX, $CH_3CH_2OCS_2K$, MW = 160.30 g·mol^{-1}) was used as a collector. Before employing, it was purified five times by recrystallisation from a petroleum ether/acetone mixture and stored in tightly closed container in a refrigerator. Aqueous solutions of KEX were freshly prepared in Milli-Q water (0.05 μS·cm^{-1} conductivity at 25 °C). As a frother, 4-methyl-2-pentanol (MIBC, $(CH_3)_2CHCH_2CH(OH)CH_3$, MW = 102.17 g·mol^{-1}, 98%) was considered in constant concentration of 25 mg·dm^{-3}, which was slightly above the value of critical coalescence concentration (CCC), determined by Karakashev et al. [28] as ca. 10 mg·dm^{-3}. The CCC can be determined as a minimum concentration of frother at which the coalescence of air bubbles is prevented [29]. In addition, Szyszka et al. [30] showed that flotation of Kupferscheifer shale was very efficient in the vicinity of CCC.

Analytically grade decahydronaphthalene ($C_{10}H_{18}$, MW = 138.25 g·mol^{-1}), supplied by Fisher Scientific, was applied as an index-matching liquid in the dynamic light scattering analysis for bubble size measurement.

Hydrochloric acid (HCl, 36.46 g·mol^{-1}) and sodium hydroxide (NaOH, 40.00 g·mol^{-1}), both supplied by Avantor Performance Materials (Poland), were used to adjust pH in zeta potential measurements.

2.3. Methods

2.3.1. Pre-treatment

The conditioning of shale was carried out by mixing 1.0 g of solid particles with 0.500 dm^3 of either water or aqueous solutions of flotation reagents on a magnetic stirrer at 300 rpm for 10 min. The MIBC concentration was constant and equal to 25 mg·dm^{-3}, while the concentration of KEX ranged from 0 to 1.0 mg·dm^{-3}. In the ultrasound pre-treatment (UPT) experiments, the ultrasound was applied to the shale suspension using an ultrasonic homogeniser Sonopuls HD 2070 (Bandelin , Germany) equipped with VS 70T sonotrode at 20 kHz frequency and power ranging from 0 to 60 W (Fig. 2A).

2.3.2. Micro-flotation experiments

After the pre-treatment (and cooling down in case of UPT) the suspension was transferred into a glass round cross-section flotation column (⌀40 mm) with a length of 40 cm (to avoid the particle entrainment) and a 10–16 μm pore size ceramic frith. During flotation the suspension was mixed with a magnetic stirrer (Fig. 2B). The flotation experiments were carried out for 5 min at the air flow rate of 25 ml·min^{-1}. After this time, no more floated material was observed in the foam layer in all tests. The floating and non-floating products were collected and dried in a vacuum dryer to determine their weights, and thus mass recoveries.

All experiments were performed at natural pH (6.0–6.5) and temperature of 22 °C. The pH of suspensions did not change in the UPT tests. All experiments were repeated three times, and the average values were presented as the ultimate results.

2.3.3. Hydrophobicity

The advancing and receding contact angles of the liquids on the flat shale surface were measured by a sessile drop method using an optical goniometer (OCA 15EC, DataPhysics Instruments GmbH, Germany). Prior to the measurement the shale surface was polished with 2000 grit sandpaper, and then rinsed with a large amount of Milli-Q® water. Then, a 1 μL liquid droplet was settled on the surface of shale and its size was changed by injection and withdrawn of a 4 μL of liquid at a 0.5 μL·s^{-1} rate. The images of droplet shape were recorded in 16 frames per second rate and analysed with the SCA 20 Software. All measurements were carried out in the saturated water vapour atmosphere. Each experiment was repeated five times at random locations of the surface, and the average values were calculated and illustrated in relevant figures.

2.3.4. Single bubble tests

The investigation of bubble interaction with the shale surface as well as bubble velocity was performed without and with UPT. The experimental setup for monitoring the dynamic phenomena occurring during the collision of a single bubble with a solid surface was described in detail elsewhere [31]. Briefly, the experimental setup consisted of a 260 mm height square cross-section (40x40mm) glass column and a heavy-walled capillary (VitroCom, USA), with an internal diameter of 0.025 mm, placed at the bottom. The flat shale sample (same as the one used for sessile drop) was mounted into a Teflon holder and placed in the glass column, filled with liquid, 250 mm above the capillary orifice. This distance is much longer than that necessary for the rising bubble to reach the terminal velocity [31]. The air bubble was generated through the capillary by a single bubble generator [32]. The UPT was applied in the same way as for shale dispersion for flotation. The process of bubble-surface interaction was recorded with a 1 ms interval using a high-speed camera (Optronis GmbH, Germany) equipped with a telecentric lens and illuminator (Sill Optics GmbH & Co. KG, Germany). Recorded images were evaluated by the image analysis in the MATLAB (MathWorks, USA) software to calculate the bubble velocity and diameter. The average bubble diameter was obtained to be of 993 ± 3 μm.

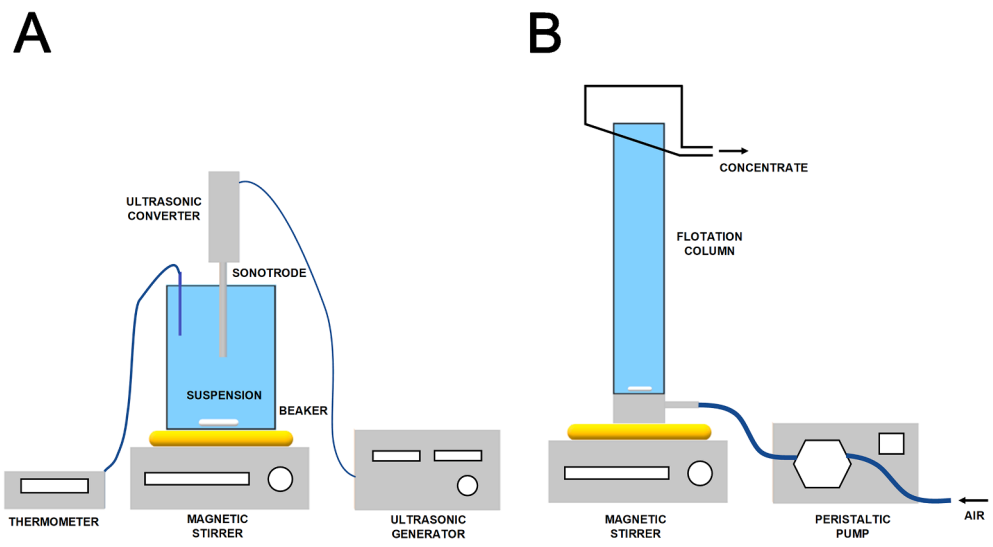

Fig. 2. Schematic pre-treatment setup of sonication process (A) and micro-flotation (B) experiments.

2.3.5. Particle size distribution

The shale particle size distribution was determined by a Mastersizer 2000 (Malvern Instruments, UK) laser diffractometer equipped with a Hydro 2000MU dispersion unit. Each measurement was conducted by dispersing a sample of shale particles in water using a dispersing unit (pump speed of 2000 rpm). The mass of added sample was determined by an obscurance parameter (the fraction of light "lost" from the analyser beam when the sample is introduced). For reliable measurements, the obscuration was maintained at ca. 10% according to the manufacturer's recommendations. The sample measurement time was set to 5 s, and five consecutive measurements were taken, from which the average value was then calculated. The values of light refraction index for continuous and dispersed phases were set as 1.33 and 1.53, respectively, and an adsorption coefficient for the dispersed phase was set to 0.1.

2.3.6. Zeta potential

The zeta potential of particles was measured with a Zetasizer 2000 (Malvern Instruments, UK) analyser. Series of suspensions of 0.010 g of shale particles (-45 μm) in 50 cm^3 of aqueous solution of KEX (0.4 $mg{\cdot}dm^{-3}$) and MIBC (25 $mg{\cdot}dm^{-3}$) were prepared. The pH of solutions was set to a desired value by either HCl or NaOH solutions. After 10 min of conditioning, the suspension was introduced in the electrophoresis cell. The value of zeta potential was determined as an average of five successive measurements.

2.3.7. Adsorption of collector

UV–visible absorption measurement was employed to determinate the amount of KEX present in liquid after UPT KEX-MIBC with and without shale. Spectra were acquired with an Evolution 201 UV–Vis spectrophotometer (Thermo Fisher, USA). Each sample of aqueous solutions was measured in the 1 cm optical path length quartz cuvette with Milli-Q water as a reference. The maximum absorption peak of KEX was at 301 nm. In the examined range of the wavelength, no effect of MIBC addition on the absorbance value was noted.

2.3.8. Bubble size distribution

The size distribution of bubbles formed by the ultrasound treatment was measured via two techniques due to the wide size range. The larger bubble sizes were determined with a Mastersizer 2000 laser diffractometer (LD). The values of light refraction index for continuous and dispersed phases were set as 1.33 and 1.00, respectively, while the absorption coefficient for dispersed phase was set to 0.1. The size of smaller bubbles was determined by employing a Photocor Complex Dynamic Light Scattering analyser (Photocor, Estonia) (DLS) equipped with a 657 nm/28 mW laser and 288-channel autocorrelator, operating in a multi-tau mode. The bubbles were generated in either pure water or aqueous solutions of reagents used, and after 5 min (to allow larger bubbles to rise to the surface of the solution so that they do not affect the measurement) the sample was placed in a 27 mm diameter round glass cell and submerged in analytical grade decahydronaphthalene (supplied by Fisher Scientific, USA), as an index-matching liquid. The scattering angle was set at 90° and temperature of measurements was 22.0 ± 0.1 °C. The data analysis was performed using the DynaLS software (Alango Ltd., Israel). Both LD and DLS measurements were carried out on a liquid containing no shale particles to ensure that both coarse and ultrasonically induced fine particles did not affect the results.

3. Results

3.1. Micro-flotation tests

The results of shale flotation tests without and with ultrasound pre-treatment of suspension are presented in Figs. 3 and 4. Before applying ultrasoundly pre-treated shale to the micro-flotation experiments, the dosage of collector (KEX) was first optimised, and the obtained results are presented in Fig. 3. As seen, when the sample was floated in the solution containing only MIBC as the frother (KEX concentration equals to 0 $mg{\cdot}dm^{-3}$) its recovery was 25%, which clearly indicates the poor floatability of shale in the absence of collector. By increasing the dosage of KEX, the shale recovery improved almost linearly, to 73% at 1.0 $mg{\cdot}dm^{-3}$.

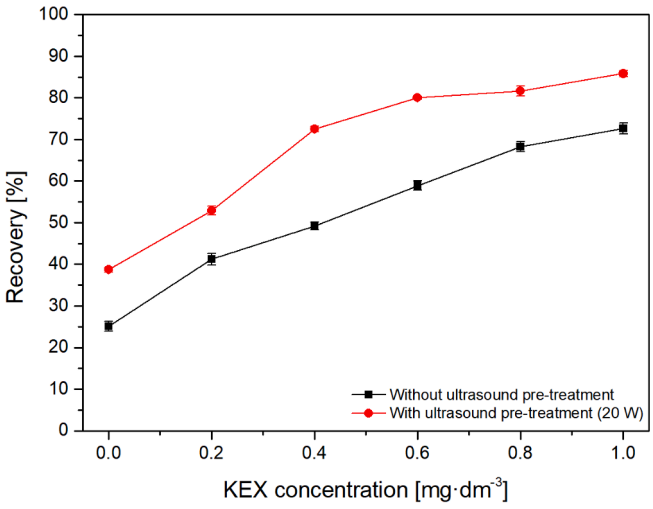

Fig. 3. Flotation recovery of shale as a function of KEX concentration (MIBC conc. = 25 $mg{\cdot}dm^{-3}$) without and with UPT (at 20 W).

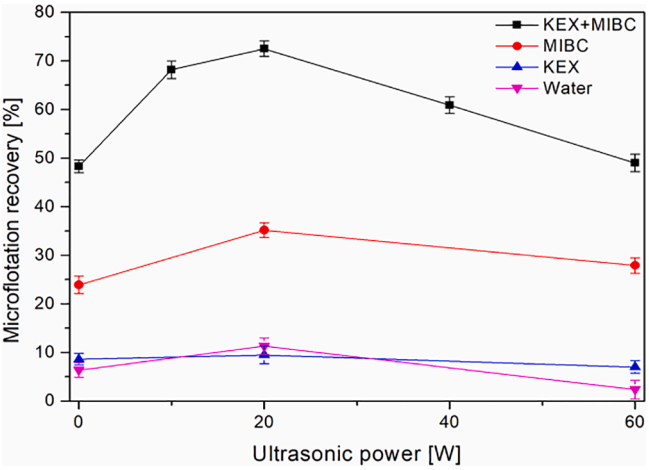

Fig. 4. Flotation recovery of shale in water, MIBC, KEX and KEX-MIBC as a function of ultrasound treatment power (KEX 0.4 $mg{\cdot}dm^{-3}$ and MIBC 25 $mg{\cdot}dm^{-3}$).

The application of UPT resulted in higher recoveries for all KEX concentrations compared to the respective values given under non-ultrasonic conditions (Fig. 3). However, the difference varied based on the KEX concentration. For example, the recovery difference observed at the concentration of 0.4 $mg{\cdot}dm^{-3}$ was the largest (equalled to 23%), while for the flotation with either no collector or its highest concentration of 1 $mg{\cdot}dm^{-3}$ the discrepancy was significantly lower, i.e., 10%. One can evidently see that the application of UPT also significantly reduces the KEX consumption. For instance, to achieve the flotation recovery of 70%, the concentration of KEX was equal to 0.4 and 1.0 $mg{\cdot}dm^{-3}$ without and with UPT, respectively. The KEX dosage of 0.4 $mg{\cdot}dm^{-3}$ resulted in the recovery of 50% (Fig. 3), for this reason, it was chosen for conducting further UPT test, since it allows to leave a margin in the recovery if the ultrasonic effect would significantly reduce or increase the flotation performance. The rest of flotation parameters were the same and kept constant.

Fig. 4 shows the influence of UPT on floatability of shale particles in

four different chemical environments i.e., only water, MIBC solution (25 mg·dm^{-3}), KEX solution (0.4 mg·dm^{-3}) and KEX-MIBC mixture. As seen, the flotation recovery of shale particles in pure water and KEX was very poor and did not exceed 10%, irrespective of UPT conditions. The addition of MIBC slightly improved the floatability of shale, however, the recovery was still very low and equal to 25% without UPT. These results also showed that floatability of shale particles in the frother solution was UPT dependent. The application of UPT at 20 W increased the recovery of shale by 10%, and then exposure to a higher power (60 W) had no significant influence on the flotation effect. The recovery was 25%, which is similar to that obtained for non-UPT conditions.

The mixture of KEX and MIBC resulted in improved recoveries because of synergistic interactions between collector and frother molecules. In this case, the application of UPT had a significant effect on the material flotation performance. The recovery increased from 50% for non-ultrasonic pre-treated to 75% at 20 W of applied power. However, the further increase in the US power led to a substantial decrease in the flotation recovery compared to 20 W, and at the highest applied power (60 W), the recovery decreased to 50%, reaching to the level of floatability of non-UPT shale. In other words, at power levels greater than 20 W, ultrasonication had a deleterious impact on the floatability of shale-bearing copper particles.

3.2. Hydrophobicity

Fig. 5 comparatively exhibits resultant advancing (θ_A) and receding (θ_R) contact angle measurements for shale in the presence of pure water, MIBC, KEX and their mixture using the sessile drop technique. As known, the θ_R appears during the formation of the bubble-particle aggregate (the TPC contact line expands causing the liquid front to recede), while the advancing angle determines its stability. Thus, the θ_R is most relevant angle to consider in analysing the particle-bubble attachment mechanism, while the θ_A for detachment. As can be evidently observed (Fig. 5), the values of θ_A are greater than θ_R under all experimental conditions. The θ_R was the least in water and slightly increased from 10° to 16° in the presence of frother, collector and their mixture. The θ_A in water was 37°, and it can be clearly seen that the addition of a flotation collector (KEX), did not change significantly its value. On the other hand, MIBC, despite being a surface active substance that accumulates mainly at the gas–liquid interface (as a frother), also has the ability to modify the hydrophobicity of shale as demonstrated by values of both θ_R and θ_A, which were higher in comparison to water and KEX. It can also be noticed that addition of KEX to MIBC solution made no significant difference in hydrophobicity of shale in comparison to sole MIBC.

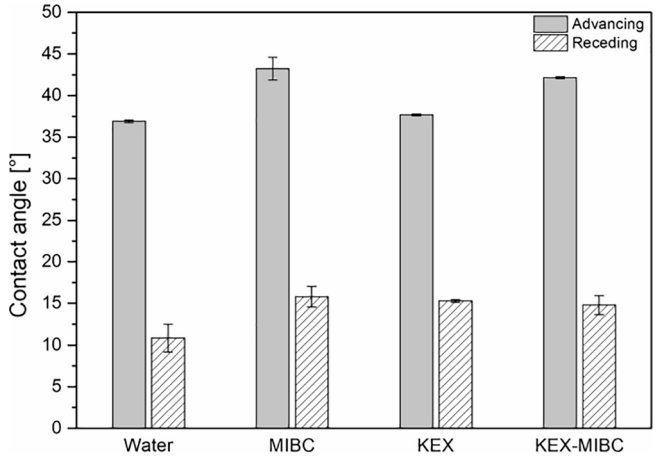

Fig. 5. Advancing (θ_A) and receding (θ_R) contact angles on shale surfaces measured by the sessile drop method (KEX 0.4 mg·dm^{-3} and MIBC 25 mg·dm^{-3}).

3.3. Particle-bubble attachment

A series of single bubble tests were performed to show the influence of UPT on kinetics of particle-bubble attachment, that is the time of three-phase contact (TPC) formation. It also allows determining the dynamic receding (θ_R) contact angle, which is essential to the quantification of mineral surface wettability and floatability. The single bubble test as a captive bubble method was preferred over the sessile-drop technique as it mimics the flotation conditions [33]. Fig. 6 shows examples of recorded images illustrating the phenomena occurring during attachment of bubble to the solid surface of shale without and with ultrasonic pre-treatment in the KEX-MIBC solution. Upon the collision with the solid surface the bubble bounced a few times, and then stayed motionless beneath the shale surface – the thin film of liquid separating the bubble and the surface did not rupture, and thus the bubble did not attach to the surface. The TPC at the shale/liquid/air interface was not formed even after 30 min. It manifests that, irrespective of UPT, the liquid film between the bubble and shale surface was very stable and did not rupture, and thus the attachment of bubble was not possible. The receding contact angle was not determined here, indicating that the shale surface did not exhibit hydrophobic properties without and with ultrasonication.

3.4. Bubble velocity

Fig. 7 displays variation in the bubble velocity in non-treated (0 W) and ultrasonically treated (20 W and 60 W) liquids viz. water and solutions of MIBC, KEX, and KEX-MIBC. As seen, without ultrasonication, bubbles in water reached to the surface with the velocity of 25 cm·s^{-1}, which is in line with the data given in the literature [34,35]. The bubble velocity in the KEX solution was almost identical as for sole water. As expected, KEX did not adsorb at the liquid–gas interface, and thus did not change the bubble velocity. Since MIBC created a retarded surface on the bubble to some extent, the bubble velocity naturally decreased from 25 to 13 cm·s^{-1}. This tendency remained constant for the bubbles in ultrasound-treated liquids with a little increase in their velocities with increasing ultrasound power.

3.5. Particle size distribution

The particle size distributions (PSDs) of shale before (0 W) and after 10 min of UPT at 20 and 60 W powers are shown in Fig. 8. As evidenced, the ultrasonic pre-treatment had a slight impact on the PSD. Even if the intensity of acoustic waves did not cause any reasonable change on the particle size reduction but it rather de-aggregated the studied sample. The ultrasonic treatment caused the appearance of finer particles, which was mainly due to the breaking effect of low frequency ultrasound. There was also an increase in the volume of medium-size particles (100 μm) for 20 W UPT, which may indicate aggregation of finer particles.

3.6. Zeta potential of shale

Fig. 9 shows the zeta potential values of shale particles measured as a function of pH in water, MIBC, and KEX-MIBC solutions before and after the ultrasonic pre-treatment. As can be seen, the zeta potential of the

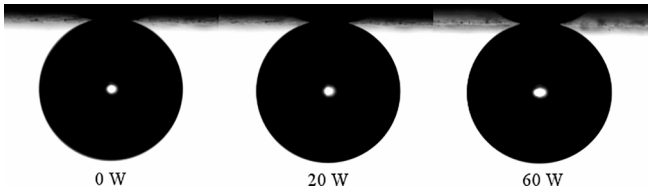

Fig. 6. Images of air bubble under the surface of shale after 0, 20 and 60 W UPT in KEX-MIBC solution (KEX 0.4 mg·dm^{-3} and MIBC 25 mg·dm^{-3}).

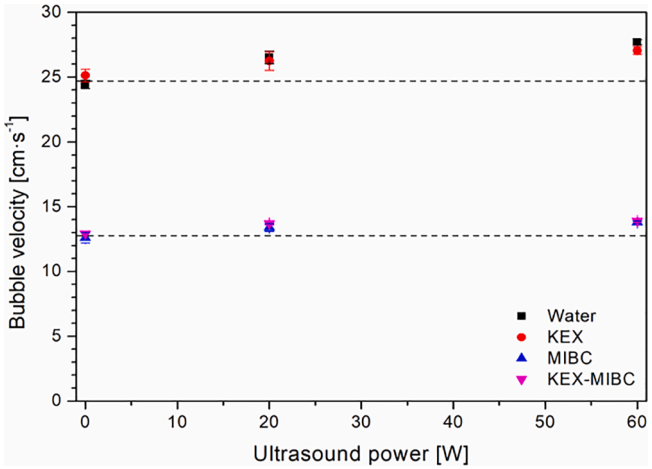

Fig. 7. Bubble velocity as a function of ultrasonication power in the presence of water, MIBC, KEX, and KEX-MIBC mixture (KEX 0.4 mg·dm^{-3} and MIBC 25 mg·dm^{-3}).

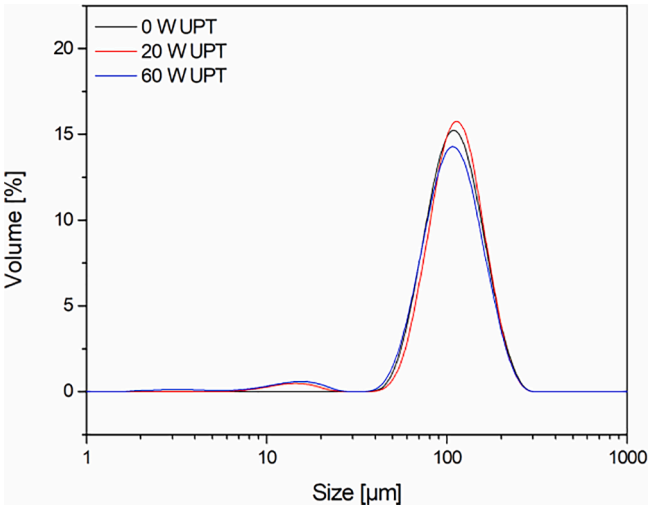

Fig. 8. Size distribution of shale particles before (0 W) and after ultrasonic pretreatments at 20 and 60 W (KEX 0.4 mg·dm^{-3} and MIBC 25 mg·dm^{-3}).

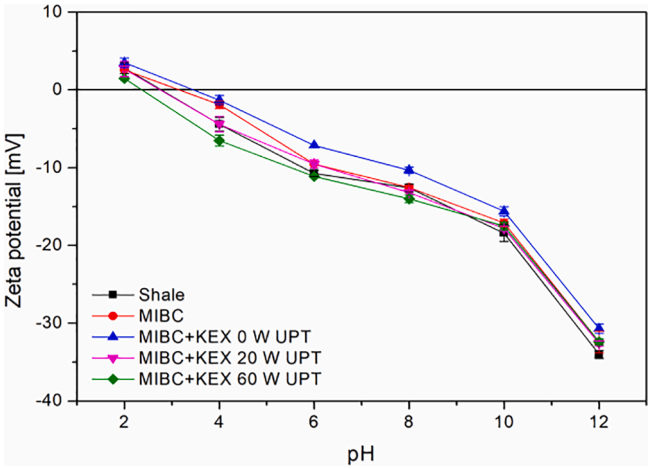

Fig. 9. Zeta potential of shale particles in water, MIBC solution (25 mg·dm^{-3}) and KEX-MIBC solution (MIBC 25 mg·dm^{-3} and KEX 0.4 mg·dm^{-3}) without and with UPT at 20 and 60 W power.

shale did not differ significantly under all conditions applied. The surface of shale was negatively charged at natural and alkaline pHs. The isoelectric point (pH_{iep}), read-off from the graph, was slightly reduced from 3.5 to 3.0 when the acoustic radiation was applied. Peng et al. [36] reported the same value of pH_{iep} (i.e., 3.5) for a similar type of mineral sample (Legnica–Glogow Copper Basin copper ore), which is in line with our findings.

3.7. Adsorption of collector

Fig. 10 shows the amount of KEX remained in the liquid after the 10 min UPT of KEX-MIBC solution without and with presence of shale, based on UV–Vis measurements. The results showed that ultrasound treatment had negligible influence on KEX molecules, the reduction of its amount in case of 20 and 60 W UPT was 2 and 3%, respectively. Therefore, it can be assumed that the decrease in the KEX amount, in the test with shale, was fully related to its adsorption on the shale particles surface. The difference in KEX adsorption on the shale, among 0, 20 and 60 W UPT, is not very significant. However, it can be seen that as the ultrasonic power increased, slightly more KEX remained in the solution. A negligible decrease in the degree of KEX adsorption at 60 W was observed as a result of increased temperature of the aqueous solution. It can be seen in Fig. 11 that the ultrasound caused almost linear increase in the liquid temperature within 10 min. At 20 W, the relative temperature increased by 4.8 °C, and for 60 W a rise of 8.4 °C was recorded.

3.8. Cavitation and generation of ultrafine bubbles

Fig. 12 illustrates the size distribution of air bubbles in aqueous solutions of MIBC and KEX after 10 min of ultrasonication. Analyses were performed using the laser diffraction analyser (LD, Fig. 12A) and dynamic light scattering (DLS, Fig. 12B). One can see that LD detected relatively large bubbles of about 1000 µm, whereas DLS displayed bubbles smaller than 1 µm. For the non-UPT solution there was a negligible amount of bubbles present in the solution, but a significant change can be observed after UPT (Fig. 12B). It was also confirmed by naked-eye observation (Fig. 12C) of scattering of the light sent through solution (the Tyndall effect). The glass column filled with the solution was illuminated by light from a telecentric illuminator ($\lambda = 632$ nm). As can be seen from the Fig. 12C, the higher the ultrasound power applied, the more intense is the light scattering and the greater amount of submicron sized bubbles in the liquid. This effect lasted for the next several days, which indicated the longevity of these small bubbles.

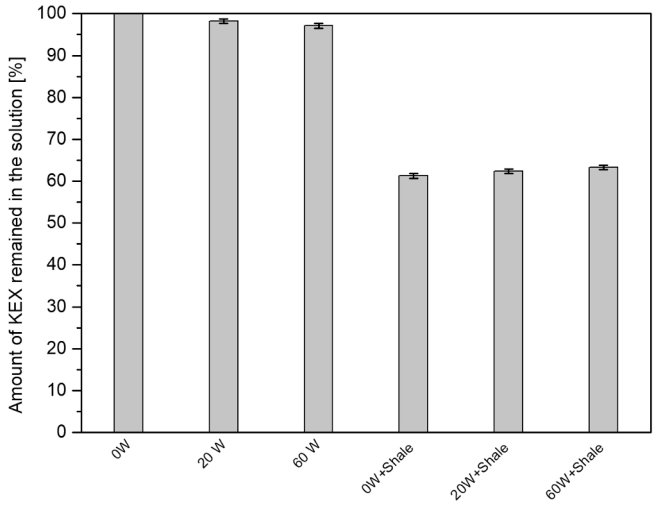

Fig. 10. The percentage of KEX remaining in solution after UPT relative to its initial amount. KEX initial concentration – 0.4 mg·dm^{-3} and MIBC concentration – 25 mg·dm^{-3}.

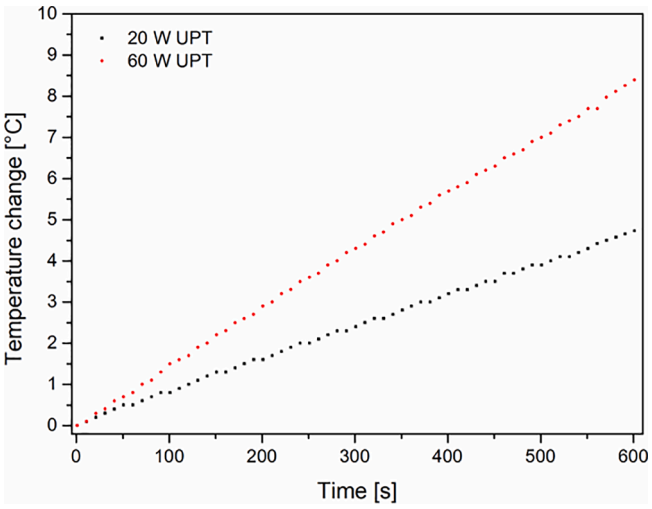

Fig. 11. Temperature change of shale suspension in KEX-MIBC solution (KEX 0.4 mg·dm^{-3}; MIBC 25 mg·dm^{-3}) during 20 and 60 W UPT.

Bubbles smaller than 1 μm can be counted as nanobubbles (NBs), also called in the literature as ultrafine bubbles [37]. It can be stated that since LD is designed and mainly applied for the particle size measurement, it may not be the appropriate technique for identifying small bubbles. The reason is ascribed to the Mie's theory, which presumes only a slight difference between the refractive indices of air bubbles and water as 1.00 and 1.33, respectively. Unlike the bubbles, particles deviate the angle of light scattered by passing through a laser beam effectively leading to substantially high accuracy of their detection compared to the bubbles. Detailed information about the advance progresses on generation, detection and application of surface nanobubbles in flotation can be found elsewhere [38-40].

4. Discussion

The obtained results of micro-flotation tests given in Fig. 4 clearly showed that there was no flotation of shale in pure water and aqueous solution of KEX. The values of isoelectric points of shale/liquid (Fig. 8) and bubble/liquid [41] interfaces were within the same range, i.e. pH_{iep} 3. Thus, in pure water and in the presence of KEX both the shale and bubble surfaces were negatively charged under the measurement condition, and repulsive electrostatic interactions prevented the liquid film rupture. The contact angles measured by the sessile drop method for water and KEX solution on the surface of shale were very similar (Fig. 5). On the other hand, the UV–Vis tests revealed that KEX molecules adsorbed on the shale surface. However, their amount was not sufficient to render the surface hydrophobicity. Low receding contact angles obtained (10-15°) classify shale as either not or poorly floatable [33]. Nevertheless, the sessile drop method did not reflect the flotation system, and the values of receding contact angles (θ_R) might be overestimated compared to the captive bubble technique. The single bubble tests (Fig. 6) showed that there was no receding contact angle, and as a result the three-phase contact at the gas-shale-solution interface was not formed, and thus effective flotation did not take place.

Flotation of shale particles was slightly improved when MIBC was added, however, the recovery was still very low and did not exceed 25%.

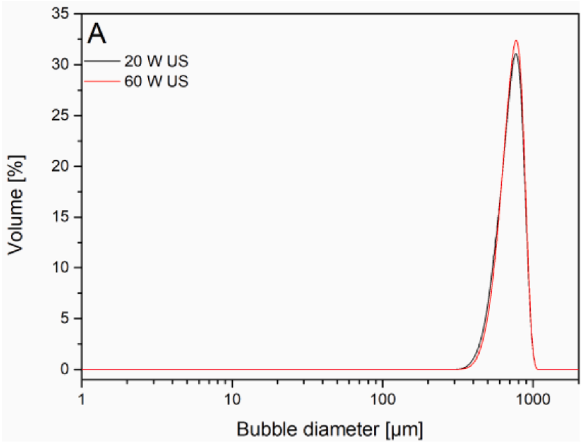

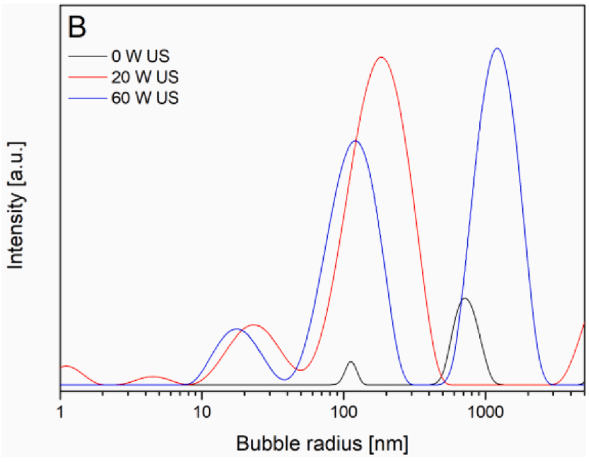

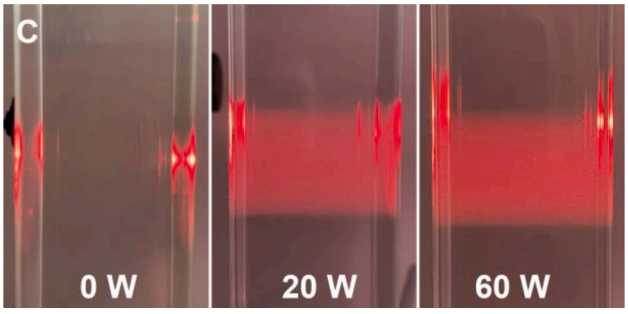

Fig. 12. Air bubble size distribution in aqueous solution of MIBC (25 mg·dm^{-3}) and KEX (0.4 mg·dm^{-3}) after 10 min sonication: obtained by A) the LD and B) DLS measurements, and C) demonstration of light scattering in solution. Fig. A), due to the inability of the instrument to measure a sample containing only liquid, does not contain data for the 0 W measurement.

Low floatability of coarse shale in the presence of frothers only was also documented elsewhere [42]. MIBC is a non-ionic surface-active substance that preferentially adsorbs at the liquid–gas interface and has an impact on the bubble size and its velocity. Therefore, MIBC affected the particle-bubble collision by increasing the sliding time between the bubble and the particle in a micro-flotation cell. It can also be found in the literature that some frothers can affect mineral hydrophobicity [42-44]. Kowalczuk et al. [42] have already demonstrated this effect for the copper-bearing shale and MIBC system. The authors state that frother enhances flotation of shale by uncovering its natural hydrophobicity, which is observed by the sessile drop measurements. In our case, MIBC slightly affected the shale hydrophobicity, which was confirmed by the obtained contact angles values. Even MIBC did not significantly change the hydrophobic state of shale, its molecules might accumulate onto the surface and, at the time of collision with bubble, re-orientate quickly and facilitate the mineral-bubble attachment [33]. Some literature suggests that molecules of MIBC can adsorb on the surface of carbonaceous matters (e.g., coal) [43], among which the shale may also be included.

As our research showed, the presence of both the frother and collector made it possible to achieve shale flotation recovery of ca. 50%. The mixture of KEX-MIBC improved the floatability as a result of synergistic interactions between their molecules. Although it was not possible to quantitively determine the interactions, the results showed that improvement in the recovery was a function of KEX concentration (Fig. 3). The interaction between the frother and collector molecules might be explained by the affinity of frother to form a hydrogen bond with the oxygen atom present in the functional group of the thiol collector (KEX). This kind of association might only be formed in the three-phase system, when the mineral is present [45]. Moreover, such interaction might preferentially take place under more turbulent conditions, what could explain why shale floated in the flotation column (dynamic process), and there was a lack of TPC formation, and thus the particle-bubble attachment in the single bubble test (nearly static process).

The results showed that the application of ultrasonic pre-treatment had a significant impact on the floatability of shale when the recovery increased by 23% at 20 W of ultrasound power (Fig. 4). As we suggest basing on literature, the improved recovery, resulting from UPT, is mainly related to: i) creation of ultrafine bubbles (NBs) on the particle surface and ii) cleaning effect through collapsing NBs. These surface fine bubbles are extremely negatively charged and have high stability (long longevity) at the particle-liquid interface having Brownian movements [46,47]. Their presence on the mineral surface plays a bridging role among conventional-sized bubble and particles leading to improvement in their floatability, as so-called secondary collector. The excessive intensity of ultrafine bubbles generated at UPT, as evidenced in Fig. 12, can lead to the formation of particle-carrier bubbles and eventually partial aggregation of particles (Fig. 8), resulting in a high probability of particle-bubble collision. These ultrafine bubbles can deposit on hydrophobic mineral surfaces, and thus improve the bubble-particle attachment efficiency [48]. In this context, Calgatoto et al. [49] proved that small NBs can enhance flotation of quartz particles by reducing the induction time. Another verification of NBs presence at the shale surface is the more negative zeta potential of particles pre-treated at 20 W in the presence of both KEX and MIBC, as shown in Fig. 9. As mentioned before, NBs are highly negatively charged.

The ultrafine bubbles have also the cleaning effect through collapsing caveated bubbles, which release a tremendous amount of pressure and temperature on particle spots. Such phenomenon removes oxidation layer and slime coatings from the shale particles and results in the production of more free, fresh and active surfaces to efficiently interact with KEX. Lastly, propagation of acoustic waves naturally creates thermal friction leading to an increase in the solution temperature [50], which was proved by the temperature measurements (Fig. 11). As known, elevated temperature may cause favourable adsorption of collector on the particle surface, which is finally associated with superior recovery [10]. In this regard, Gungoren et al. [51] investigated the effect of temperature during ultrasonic conditioning for the quartz-amine flotation. They claimed that the increase in the flotation recovery could be associated with the increase of amine molecules activities with temperature, and further the decrease caused by extremely turbulent conditions in suspension. We observed a similar decline in recovery when the power exceeded 20 W, at which the maximum recovery appeared (Fig. 4).

The micro-flotation results in the function of KEX concentration (without and with 20 W UPT) revealed that ultrasonic pre-treatment led to a significantly lower collector consumption (Fig. 3). Actually, the influence of ultra-fine bubbles generated by acoustic cavitation as a secondary collector has been verified. At least a 50% reduction in collector consumption for galena/xanthate system was reported by Celik [52] as a result of ultrasonic pre-treatment under appropriate conditions. It is most likely that nanobubbles can act like a collector making a bridge among conventional bubbles and fine particles leading to the decrease in the collector dosage requirement. Detailed information regarding such phenomenon is presented elsewhere [53].

The comparative results of dynamic light scattering at 0, 20 and 60 W powers (Fig. 12B) proved that there was no ultrafine bubble without ultrasonication (0 W), however, 20 W created a reasonable amount of such bubbles, which was lowered at 60 W. The worsened floatability of shale for higher power of UPT might be related to the lower intensity (and thus concentration) of ultrafine bubbles (NBs) as well as creation of micron-sized bubbles (MBs), which was most probably related to the coalescence of NBs and caveated transient bubble with low stabilities.

In addition to that, as reported in the literature, the longer sonication and higher power levels might facilitate the formation of OH radicals interacting with water molecules and eventually the production of hydrogen peroxides (H_2O_2) through a thermal decomposition process [9]. The H_2O_2 is a strong oxidant agent capable of oxidising copper surface, reducing its hydrophobicity and at last diminishing its recoverability. Although, as aforementioned stated, the elevated temperature might cause favourable adsorption of collector on the surface, excessive temperature might accelerate the desorption of collector from the surface. Breitbach et al. [54], who investigated the effect of ultrasound on the adsorption and desorption processes, reported that the ultrasound promoted desorption due to heat generated as a result of the ultrasonic energy dissipation. The mechanism of KEX action as a collector in the sulphide flotation is based on either the physical adsorption or the formation of insoluble sulphates on the surface of the mineral. Gurpinar et al. [48] claimed that hydrodynamic turbulence created by ultrasonic treatment can easily break the physical bonds between the collector and the mineral surface.

5. Conclusions and perspectives

The objective of this study was to determine the influence of ultrasound pre-treatment on the floatability of carbonaceous copper-bearing shale particles. Series of experiments were conducted applying ultrasound power from 0 to 60 W.

The application of UPT at 20 W resulted in higher mass recoveries of shale from 50% (without ultrasonic pre-treatment) to 75%. It was mainly related to generation of ultrafine bubbles on the solid surface and cleaning effect. Nevertheless, exceeding the ultrasonication power from 20 W to 60 W led to reduction in the floatability most likely due to the creation of H_2O_2 as a consequence of ultrasonically produced free H and OH radicals. In addition, micro-flotation tests of ultrasound pre-treated material approved over 50% reduction in the collector (KEX) consumption.

Considering the given practical results in this work and existing information in the literature, the following future works were highlighted to be worth to further investigations:

- Very limited information is known about the effect of ultrasonication power on the particle surface and its roughness. Further in-depth studies are required to clarify this in future.
- Stability of generated NBs in terms of acoustic cavitation in bulk and particle surfaces still needs more clarification to be well understood especially in terms of their detection.
- Although beneficial impact of acoustic waves has been known for a few decades and proven in this work, there is a considerable lack of practical trials in both pilot and industrial scales.
- Still it remains unknown in the literature that to which extent the minerals can be dissolved as a function of ultrasound power.

Addressing these issues will help to better understand the impact of ultrasound on flotation.

CRediT authorship contribution statement

Mateusz Kruszelnicki: Conceptualization, Methodology, Data curation, Investigation, Writing – original draft, Writing – review & editing. **Ahmad Hassanzadeh:** Writing – original draft, Writing – review & editing. **Krzysztof Jan Legawiec:** Investigation, Data curation, Writing – original draft. **Izabela Polowczyk:** Resources, Writing – original draft, Writing – review & editing, Supervision. **Przemyslaw B. Kowalczuk:** Writing – original draft, Writing – review & editing, Supervision.

Declaration of Competing Interest

The authors declare that they have no known competing financial interests or personal relationships that could have appeared to influence the work reported in this paper.

Acknowledgments

The work was financed by a subsidy from the Polish Ministry of Education and Science for Wroclaw University of Science and Technology.

References

[1] V.K. Tyagi, S.-L. Lo, L. Appels, R. Dewil, Ultrasonic Treatment of Waste Sludge: A Review on Mechanisms and Applications, Crit. Rev. Environ. Sci. Technol. 44 (11) (2014) 1220–1288, https://doi.org/10.1080/10643389.2013.763587.
[2] S. Kentish, M. Ashokkumar, The Physical and Chemical Effects of Ultrasound, in: H. Feng, G. Barbosa-Canovas, J. Weiss (Eds.), Ultrasound Technologies for Food and Bioprocessing, Springer, New York, NY, New York, NY, 2011, pp. 1–12. https://doi.org/10.1007/978-1-4419-7472-3_1.
[3] C. Aldrich, D. Feng, Effect of ultrasonic preconditioning of pulp on the flotation of sulphide ores, Miner. Eng. 12 (6) (1999) 701–707, https://doi.org/10.1016/S0892-6875(99)00053-9.
[4] C. Li, L. Dong, H. Zhang, Recovery of clean coal from tailings by flotation with aid of ultrasonic, Energy Sources Part A 40 (3) (2018) 373–379, https://doi.org/10.1080/15567036.2017.1422057.
[5] U. Malayoglu, S.G. Ozkan, Effects of Ultrasound on Desliming Prior to Feldspar Flotation, Minerals 9 (2019) 784. https://doi.org/10.3390/MIN9120784.
[6] A.R. Videla, R. Morales, T. Saint-Jean, L. Gaete, Y. Vargas, J.D. Miller, Ultrasound treatment on tailings to enhance copper flotation recovery, Miner. Eng. 99 (2016) 89–95, https://doi.org/10.1016/J.MINENG.2016.09.019.
[7] Y. Chen, V.N.T. Truong, X. Bu, G. Xie, A review of effects and applications of ultrasound in mineral flotation, Ultrason. Sonochem. 60 (2020) 104739.
[8] A. St. Slaczka, Effects of an ultrasonic field on the flotation selectivity of barite from a barite-fluorite-quartz ore, Int. J. Miner. Process. 20 (1987) 193–210, https://doi.org/10.1016/0301-7516(87)90066-4.
[9] W.-z. Kang, H.-X. Xun, X.-H. Kong, M.-M. Li, ming Li, Effects from changes in pulp nature after ultrasonic conditioning on high-sulfur coal flotation, Mining Sci. Technol. (China) 19 (4) (2009) 498–507, https://doi.org/10.1016/S1674-5264(09)60093-4.
[10] C. Gungoren, O. Ozdemir, X. Wang, S.G. Ozkan, J.D. Miller, Effect of ultrasound on bubble-particle interaction in quartz-amine flotation system, Ultrason. Sonochem. 52 (2019) 446–454, https://doi.org/10.1016/J.ULTSONCH.2018.12.023.
[11] A. Hassanzadeh, H. Gholami, S.G. Özkan, T. Niedoba, A. Surowiak, Effect of Power Ultrasound on Wettability and Collector-Less Floatability of Chalcopyrite, Pyrite and Quartz, Minerals 11 (2021) 48. https://doi.org/10.3390/MIN11010048.
[12] Ş.G. Özkan, H.Z. Kuyumcu, Design of a flotation cell equipped with ultrasound transducers to enhance coal flotation, Ultrason. Sonochem. 14 (5) (2007) 639–645.
[13] E.C. Cilek, S. Ozgen, Effect of ultrasound on separation selectivity and efficiency of flotation, Miner. Eng. 22 (14) (2009) 1209–1217.
[14] A. Hassanzadeh, S.A. Sajjady, H. Gholami, S. Amini, S.G. Özkan, An Improvement on Selective Separation by Applying Ultrasound to Rougher and Re-Cleaner Stages of Copper Flotation, Minerals 10 (2020) 619. https://doi.org/10.3390/MIN10070619.
[15] K. Yasuda, H. Matsushima, Y. Asakura, Generation and reduction of bulk nanobubbles by ultrasonic irradiation, Chem. Eng. Sci. 195 (2019) 455–461, https://doi.org/10.1016/J.CES.2018.09.044.
[16] C. Li, X. Li, M. Xu, H. Zhang, Effect of ultrasonication on the flotation of fine graphite particles: Nanobubbles or not? Ultrason. Sonochem. 69 (2020) 105243.
[17] Q. Cao, J. Cheng, Q. Feng, S. Wen, B. Luo, Surface cleaning and oxidative effects of ultrasonication on the flotation of oxidized pyrite, Powder Technol. 311 (2017) 390–397, https://doi.org/10.1016/J.POWTEC.2017.01.069.
[18] S.D. Barma, P.K. Baskey, D.S. Rao, S.N. Sahu, Ultrasonic-assisted flotation for enhancing the recovery of flaky graphite from low-grade graphite ore, Ultrason. Sonochem. 56 (2019) 386–396, https://doi.org/10.1016/J.ULTSONCH.2019.04.033.
[19] S.G. Ozkan, H.Z. Kuyumcu, Investigation of mechanism of ultrasound on coal flotation, Int. J. Miner. Process. 81 (3) (2006) 201–203.
[20] S.G. Ozkan, Effects of simultaneous ultrasonic treatment on flotation of hard coal slimes, Fuel 93 (2012) 576–580, https://doi.org/10.1016/J.FUEL.2011.10.032.
[21] W. Kang, H. Li, Enhancement of flaky graphite cleaning by ultrasonic treatment, R. Soc. Open Sci. 6 (12) (2019) 191160.
[22] H. Ebrahimi, M. Karamoozian, Effect of ultrasonic irradiation on particle size, reagents consumption, and feed ash content in coal flotation, Int. J. Coal Sci. Technol. 7 (2020) 787–795, https://doi.org/10.1007/S40789-020-00307-2/FIGURES/6.
[23] M. Xu, C. Li, H. Zhang, N. Kupka, U.A. Peuker, M. Rudolph, A contribution to exploring the importance of surface air nucleation in froth flotation – The effects of dissolved air on graphite flotation, Colloids Surf., A 633 (2022) 127866.
[24] A.M. Gaudin, J.O. Groh, H.B. Henderson, Effect of particle size on flotation, AIME Technical Publications 414 (1931) 3–23.
[25] G.J. Jameson, A.v. Nguyen, S. Ata, The flotation of fine and coarse particles, in: M. C. Fuerstenau, G. Jameson, R.-H. Yoon (Eds.), Froth Flotation a Century of Innovation, Society for Mining, Metallurgy, and Exploration, Inc., Shaffer Parkway, 2007, pp. 339–372.
[26] A. Rahfeld, R. Kleeberg, R. Möckel, J. Gutzmer, Quantitative mineralogical analysis of European Kupferschiefer ore, Miner. Eng. 115 (2018) 21–32, https://doi.org/10.1016/J.MINENG.2017.10.007.
[27] S.M. Bulatovic, Handbook of Flotation Reagents: Chemistry, Theory and Practice Flotation of Sulfide Ores, Elsevier (2007), https://doi.org/10.1016/B978-0-444-53029-5.X5009-6.
[28] S.I. Karakashev, N.A. Grozev, K. Batjargal, O. Guven, O. Ozdemir, F. Boylu, M.S. Çelik, Correlations for Easy Calculation of the Critical Coalescence Concentration (CCC) of Simple Frothers, Coatings 10 (2020) 612. https://doi.org/10.3390/COATINGS10070612.
[29] Y.S. Cho, J.S. Laskowski, Effect of flotation frothers on bubble size and foam stability, Int. J. Miner. Process. 64 (2-3) (2002) 69–80, https://doi.org/10.1016/S0301-7516(01)00064-3.
[30] D. Szyszka, P. Pazik, A. Zwierzchowska, Flotacja łupka miedzionośnego w obecności eterów butylowo-etylenoglikolowego i butylowo-dwuetylenoglikolowego, in: J. Drzymala, P.B. Kowalczuk (Eds.), Łupek Miedzionośny, Wydział Geoinżynierii, Górnictwa i Geologii, Politechnika Wrocławska, Wroclaw, 2014, pp. 103–106.
[31] J. Zawala, J. Drzymala, K. Malysa, An investigation into the mechanism of the three-phase contact formation at fluorite surface by colliding bubble, Int. J. Miner. Process. 88 (3-4) (2008) 72–79.
[32] J. Zawala, A. Niecikowska, "Bubble-on-demand" generator with precise adsorption time control, Rev. Sci. Instrum. 88 (9) (2017) 095106, https://doi.org/10.1063/1.5001846.
[33] J.W. Drelich, A. Marmur, Meaningful contact angles in flotation systems: critical analysis and recommendations, Surf. Innov. 6 (2018) 19–30, https://doi.org/10.1680/JSUIN.17.00037.
[34] A. Sam, C.O. Gomez, J.A. Finch, Axial velocity profiles of single bubbles in water/frother solutions, Int. J. Miner. Process. 47 (3-4) (1996) 177–196, https://doi.org/10.1016/0301-7516(95)00088-7.
[35] A. Hassanzadeh, B.V. Hassas, S. Kouachi, Z. Brabcova, M.S. Çelik, Effect of bubble size and velocity on collision efficiency in chalcopyrite flotation, Colloids Surf., A 498 (2016) 258–267, https://doi.org/10.1016/J.COLSURFA.2016.03.035.
[36] M. Peng, T. Ratajczak, J. Drzymała, Zeta potential of Polish copper-bearing shale in the absence and presence of flotation frothers, Mining Sci. 21 (2014) 57–63, https://doi.org/10.5277/MS142105.
[37] S. Nazari, S.Z. Shafaei, A. Hassanzadeh, A. Azizi, M. Gharabaghi, R. Ahmadi, B. Shahbazi, Study of effective parameters on generating submicron (nano)-bubbles using the hydrodynamic cavitation, Physicochem. Probl. Miner. Process. 56 (2020) 884–904. https://doi.org/10.37190/PPMP/126628.
[38] C. Li, H. Zhang, Surface nanobubbles and their roles in flotation of fine particles – A review, J. Ind. Eng. Chem. 106 (2022) 37–51, https://doi.org/10.1016/J.JIEC.2021.11.009.
[39] C. Li, H. Zhang, A review of bulk nanobubbles and their roles in flotation of fine particles, Powder Technol. 395 (2022) 618–633, https://doi.org/10.1016/J.POWTEC.2021.10.004.

[40] F. Zhang, L. Sun, H. Yang, X. Gui, H. Schönherr, M. Kappl, Y. Cao, Y. Xing, Recent advances for understanding the role of nanobubbles in particles flotation, Adv. Colloid Interface Sci. 291 (2021) 102403.
[41] U.T. Gonzenbach, A.R. Studart, E. Tervoort, L.J. Gauckler, Stabilization of Foams with Inorganic Colloidal Particles, Langmuir 22 (26) (2006) 10983–10988.
[42] P.B. Kowalczuk, D. Mroczko, J. Drzymala, Influence of frother type and dose on collectorless flotation of copper-bearing shale in a flotation column, Physicochem. Probl. Miner. Process. 51 (2015) 547–558, https://doi.org/10.5277/PPMP150215.
[43] L. Cao, X. Chen, Y. Peng, The adsorption and orientation of frother surfactants on heterogeneous wetting surfaces, Appl. Surf. Sci. 548 (2021) 149225.
[44] Y. Chen, H. Li, D. Feng, X. Tong, S. Hu, F. Yang, G. Wang, A recipe of surfactant for the flotation of fine cassiterite particles, Miner. Eng. 160 (2021) 106658.
[45] J. Leja, Interactions of surfactants, Miner. Process. Extr. Metall. Rev. 5 (1989) 1–22.
[46] M. Fan, D. Tao, R. Honaker, Z. Luo, Nanobubble generation and its application in froth flotation (part I): nanobubble generation and its effects on properties of microbubble and millimeter scale bubble solutions, Mining Sci. Technol. (China) 20 (1) (2010) 1–19, https://doi.org/10.1016/S1674-5264(09)60154-X.
[47] S. Nazari, A. Hassanzadeh, The effect of reagent type on generating bulk sub-micron (nano) bubbles and flotation kinetics of coarse-sized quartz particles, Powder Technol. 374 (2020) 160–171, https://doi.org/10.1016/J.POWTEC.2020.07.049.
[48] G. Gurpinar, E. Sonmez, V. Bozkurt, Effect of ultrasonic treatment on flotation of calcite, barite and quartz, Mineral Process. Extract. Metall. 113 (2) (2004) 91–95, https://doi.org/10.1179/037195504225005796.
[49] S. Calgaroto, A. Azevedo, J. Rubio, Flotation of quartz particles assisted by nanobubbles, Int. J. Miner. Process. 137 (2015) 64–70, https://doi.org/10.1016/J.MINPRO.2015.02.010.
[50] K.S. Suslick, The chemical effects of ultrasound, Sci. Am. 260 (2) (1989) 80–86.
[51] C. Gungoren, O. Ozdemir, S.G. Ozkan, Effects of temperature during ultrasonic conditioning in quartz-amine flotation, Physicochem. Probl. Miner. Process. 53 (2017) 687–698, https://doi.org/10.5277/PPMP170201.
[52] M.S. Celik, Effect of Ultrasonic Treatment on the Floatability of Coal and Galena, Sep. Sci. Technol. 24 (14) (1989) 1159–1166, https://doi.org/10.1080/01496398908049894.
[53] N.N. Rulyov, D.Y. Sadovskiy, N.A. Rulyova, L.O. Filippov, Column flotation of fine glass beads enhanced by their prior heteroaggregation with microbubbles, Colloids Surf., A 617 (2021) 126398.
[54] M. Breitbach, D. Bathen, H. Schmidt-Traub, Effect of Ultrasound on Adsorption and Desorption Processes, Ind. Eng. Chem. Res. 42 (22) (2003) 5635–5646.